Research Square

Preprints are preliminary reports that have not undergone peer review.
They should not be considered conclusive, used to inform clinical practice,
or referenced by the media as validated information.

ZrO_2 Negtive Capacitance Field-Effect Transistor with Sub-60 Subthreshold Swing Behavior

Siqing Zhang
Xidian University
Huan Liu
Xidian University
Jiuren Zhou
Xidian University
Yan Liu (xidianliuyan@xidian.edu.cn)
Xidian University School of Microelectronics https://orcid.org/0000-0003-4724-6588
Genquan Han
Xidian University School of Microelectronics
Yue Hao
Xidian University School of Microelectronics

Nano Express

Keywords: Amorphous ZrO2, Ferroelectric, FET, Subthreshold Swing, Negative Capacitance

Posted Date: October 6th, 2020

DOI: https://doi.org/10.21203/rs.3.rs-77514/v1

License: This work is licensed under a Creative Commons Attribution 4.0 International License.
Read Full License

Version of Record: A version of this preprint was published at Nanoscale Research Letters on February 2nd, 2021. See the published version at https://doi.org/10.1186/s11671-020-03468-w.

Abstract

Here we report the ZrO2 - based Negative capacitance (NC) FETs with 45.06 mV/decade subthreshold swing (SS) under ±1 V V GS range, which can achieve new opportunities in furture voltage-scalable NCFET applications. The ferroelectric-like behavior of the Ge/ZrO2/TaN capacitors is proposed to be originated from the oxygen vacancy dipoles. The NC effect of the amorphous HfO2 and ZrO2 films devices can be proved by the sudden drop of gate leakage, the negative differential resistance (NDR) phenomenon, the enhancement of I DS and sub-60 subthreshold swing. 5 nm ZrO2 - based NCFETs achieve a clockwise hysteresis of of 0.24 V, lower than 60 mV/decade SS and an 12% I DS enhancement compared to the control device without ZrO2 . The suppressed NC effect of Al2O3/HfO2 NCFET compared with ZrO2 NCFET is related to the partical swiching of oxygen vacancy dipoles in the forward sweeping due to negative interfical dipoles at the Al2O3 /HfO2 interface.

Background

As complementary metal oxide semiconductor (CMOS) devices scaling down constantly, the integrated circuit (IC) technique has entered into the era of “more than Moore era”. The driving force of IC industry and technology becomes the reduction of power consumption, instead of the miniaturization of transistors [1,2]. However, the Boltzmann tyranny of MOSFETs, more than 60 mV/decade SS has restricted the energy/power effificiency [3]. In recent years, many proposed novel devices have the ability to achieve sub−60 mV/decade threshold swing, including impact ionization MOSFETs, tunnel FETs and NCFETs [4–7]. Due to the simple structure, the steep SS and imporved drive current, NCFETs with a ferroelectric (FE) film have been regarded as an attractive alternative among these emerging devices [8–10]. The reported experiments on NCFETs mainly include $PbZrTiO_3$ (PZT), P(VDF-TrFE) and $HfZrO_x$ (HZO) [11–17]. Even though the ferroelectricity of these materials satisfies the requirement of the state-of-the-art technology nodes [18], the relatively high remant polarization (P_r) and coercive filed (E_c) lead to rather strong depolarization and much high power consumption [19–26]. Recently, ferroelectricity in the amorphous Al_2O_3 and ZrO_2 filmsenabled bythe voltage-modulated oxygen vacancy dipoleshas been investigated [27–29]. This enables mass experiments about ZrO_2-based FeFET for nonvoile memory and analog synapse applications [30–35]. However, the systematical investigation on one-transistor ZrO_2-based NCFET has not been carried out.

In this work, Ge NCFETs with 5 nm ZrO_2 ferroelectric dielectric layer and 5 nm Al_2O_3/HfO_2 ferroelectric dielectric layer have been proposed, respectively. We experimentally observed sub−60 mV/decade steep slope in ZrO_2 (5 nm) NCFET, which can be attributed to the NC effect of ZrO_2 ferroelectric layer. And we analyzed the polrazation P as function of applied voltage V for the Ge/ZrO_2/TaN capacitors. The ferroelectric-like behavior of the Ge/ZrO_2/TaN capacitors is induced by the voltage-induced oxygen vacancy dipoles. Moreover, we attributed the improved I_{DS} and the sudden drop of I_G in the Al_2O_3/HfO_2 NCFETs and ZrO_2 NCFETs to the NC effect. We also observed the NDR phenomenon in the Al_2O_3/HfO_2 NCFETs and ZrO_2 NCFETs. In addition, we further analyzed the physical mechanism of interfical dipoles-

induced decreased NC effect in the Al_2O_3/HfO_2 NCFET. The ZrO_2 NCFETs with sub–60 mV/decade steep slope, improved drain voltage and low operating voltage will be suit for the design of NCFETs with low power consumption in the “more than Moore era”.

Methods

Key process steps for NCFETs with ZrO_2 and Al_2O_3/HfO_2 fabrication are shown in Fig. 1 (a). Different gate dielectric insulators, including Al_2O_3/ amorphous HfO_2 (5 nm) films and amorphous ZrO_2 (4.2 nm)films were grown on n-Ge (001) substrates by atomic layer deposition (ALD) at 300 ^oC. TMA, TDMAHf, TDMAZr and H_2O vapor were used as the precursors of Al, Hf, Zr and O, respectively. A TaN top gate electrode was then deposited on HfO_2 orZrO_2 surfaces by reactive sputtering. Source/drain (S/D) regions were defined by lithography patterning and dry etching. After that, source/drain (S/D) regions were implanted with boron (B^+) and nickel (Ni) was deposited in source/drain (S/D) regions. Finally, rapid thermal annealing (RTA) at 350 ^oC for 30 s was carried out. Fig. 1 (b) and (d) show the schematics of the fabricated Al_2O_3/HfO_2 NCFETs and ZrO_2 NCFETs. High-resolution transmission electron microscope (HRTEM) image in Fig. 1 (c) depicts the amorohous HfO_2 (5 nm) film on Ge(001) with Al_2O_3 interfacial layer. HRTEM image in Fig. 1 (e) depicts the amorohous ZrO_2 (4.2 nm) film on Ge (001).

Results And Discussion

Fig. 2 (a) shows the measured curves of polarization *P v.s.* applied voltage *V* characteristics for the $Ge/ZrO_2/TaN$ capacitors at 3.3 kHz. The gate length (L_G) of the capacitors are 8 μm. It is observed that the P_r of the $Ge/ZrO_2/TaN$ capacitors can be enhanced with larger sweeping range of *V.* The ferroelectric-like behavior of the amorphous ZrO_2 film in the Fig. 2 (a) is proposed to be originated from the oxygen vacancy dipoles [36]. Fig. 2 (b) shows the measured *P-V* curves for the $Ge/ZrO_2/TaN$ capacitors under different frequencies from 200 Hz to 10 k Hz. We can see that the ferroelectric-like behaviorof the amorphous ZrO_2 film remain stable for all frequencies. However, the P_r of the amorphous ZrO_2 film is reduced with the increased frequencies. This phenomenon can be explained by the incomplete dipoles switching under high measurement frequencies [37,38].

Fig. 3 (a) shows the measured I_{DS}-V_{GS} curves of a ferroelectric Al_2O_3/HfO_2 NCFET at the V_{DS} of - 0.05 V and - 0.5 V. The L_G of the devices are 3 μm. The hysteresis loops of 0.14 V (V_{ds} = - 0.05 V, I_{ds} = 1 nA/μm) and 0.08 V (V_{ds} = - 0.5 V, I_{ds} = 1 nA/μm) are demonstrated, respectively. The clockwise hysteresis loops are attributed to the migration of oxygen vacancies and accompanied negative charges. The oxygen vacancy dipoles accumulate (deplete) in the Ge/Al_2O_3 interface under positive (negative) V_{GS}. Therefore, the threshold voltage (V_{TH}) increases (decreases) under forward (reverse) sweeping of gate voltages. As shown in Fig. 3 (b), the output characteristics of the Al_2O_3/HfO_2 NCFET and the control FET are compared. The saturation current of the Al_2O_3/HfO_2 NCFET exceeds 26 μA/μm, with a rise of 23 % compared to that of the control FET at $|V_{GS}\text{-}V_{TH}| = |V_{DS}|$ = 0.8 V. The current enhancement is induced by

the increased inversion charge intensity (Q_{inv}) in the reverse polarization electric field and the amplication of surface potential [39,40]. In addition to current enhancement, the obtained obvious NDR proves the NC effect of the amorphous HfO_2 film. The NDR effect is caused by the incomplete switching of oxygen vacancy dipoles due to the coupling of drain-to-channel as V_{DS} increases [41,42]. Fig. 3 (c) compares the measured gate leakage I_G-V_{GS} curves for the 5 nm Al_2O_3/HfO_2 NCFET at the V_{DS} of - 0.05 V and –0.5 V. The sudden drops of I_G onlyduring the reverse sweeping indicate the decreased voltage in the amorphous HfO_2 film and the amplication of surface potential [43]. The absence of NC effect during the forward sweeping is caused by the partical switching of oxygen vacancy dipoles in the amorphous HfO_2 film [44]. The different ability to contain oxygen atoms between Al_2O_3 and HfO_2 layer leads to oxygen redistribution and negative interfacial dipoles at the Al_2O_3/HfO_2 interface [45–47]. Due to the presense of negative interfacial dipoles, it is difficult for the amorphous HfO_2 film to realize complete polarization swiching (NC effect) in the forward sweeping.

Fig. 4 (a) shows the measured transfer curves of a ferroelectric ZrO_2 NCFET at the V_{DS} of - 0.05 V and - 0.5 V. The L_G of the two devices are 4 μm. The clockwise hysteresis loops of 0.24 V (V_{ds} = - 0.05 V, I_{ds} = 1 nA/μm) and 0.14 V (V_{ds} = - 0.5 V, I_{ds} = 1 nA/μm) are demonstrated, respectively. As shown in Fig. 4 (b), the output characteristics of the ZrO_2 NCFET and the control FET are compared. The saturation current of the ZrO_2 NCFET exceeds 30 μA/μm, with a rise of 12 % compared to that of the control FET at $|V_{GS}$-$V_{TH}|$ = $|V_{DS}|$ = 1 V. The improved current enhancement and more obvious NDR indicate the enhanced NC effect of the amorphous ZrO_2 film (5 nm) contrast to that of 5 nm HfO_2 film. Fig. 3 (c) compares the measured gate leakage I_G-V_{GS} curves for the 5 nm ZrO_2 NCFET at the V_{DS} of - 0.05 V and - 0.5 V. Compared to the sudden I_G drops of Al_2O_3/HfO_2 NCFET only during reverse sweeping in Fig. 3 (c), the sudden drops of I_G both in forward and reverse sweeping also prove the enhanced NC effect in the amorphous ZrO_2 film.

Fig. 5 (a) and (b) shows the point SS as function of I_{DS} for the Al_2O_3/HfO_2 and ZrO_2 NCFET at the V_{DS} of - 0.05 V and - 0.5 V. Sub–60 mV/decade subthreshold swing (SS) can be achieved during forward or reverse sweeping of V_{GS} at the V_{DS} of - 0.05 V and - 0.5 V. When V_{DS} is - 0.05 V, a point forward SS of 45.1 mV/dec and a point reverse SS of 55.2 mV/dec were achieved. When V_{DS} is - 0.5 V, a point forward SS of 51.16 mV/dec and a point reverse SS of 46.52 mV/dec were achieved. Due to the different ability of scavenging effect for the Al_2O_3/HfO_2 and ZrO_2 layer, the partical dipoles switching is caused in the Al_2O_3/HfO_2 NCFET. Therefore, the more obvious NC effect with sub–60 mV/decade SS is achieved in 5 nm ZrO_2 NCFET.

Conclusions

We report the demonstration of ferroelectric NC ZrO_2 pFETs with the sub–60 mV/decade SS, low operating voltage of 1 V and a hysteresis of less than 60 mV. The impact of the amorphous ZrO_2 films on the ferroelectric behavior is explained by the oxygen vacancy dipoles. The improved I_{DS} and NDR

phenomenon are also obtained in Al_2O_3/HfO_2 NCFETs and ZrO_2 NCFETs compared to the control device. The suppressed NC effect of the Al_2O_3/HfO_2 NCFET can be attributed to partical dipole swiching due to interfical dipoles at the Al_2O_3/HfO_2 interface. The ZrO_2 NCFETs with sub−60 mV/decade steep slope, improved drain voltage and low operating voltage pave a new way for future low power consumption NCFETs design.

Abbreviations

TaN: Tantalum nitride; ZrO_2: Zirconium dioxide; ; TDMAZr: Tetrakis (dimethylamido) zirconium; P_r: remnant polarization; E_c: coercive electric field; MOSFETs: Metal-oxide-semiconductor field-effect transistors; Ge: Germanium; ALD: Atomic layer deposition; B^+: Boron ion; Al_2O_3: aluminum oxide; HRTEM: High-resolution transmission electron microscope; Ni: Nickel; RTA: repaid thermal annealing; I_{DS}: drain current; V_{GS}: gate voltage; V_{TH}: threshold voltage; NCFET: negative capacitance field-effect transistor.

Declarations

Acknowledgments

Not applicable.

Funding

The authors acknowledge support from the National Key Research and Development Project (Grant No. 2018YFB2202800, 2018YFB2200500, and 2018YFA0307300) and the National Natural Science Foundation of China (Grant No. 61534004, 91964202, 61874081, 61851406, and 61775092).

Competing interests

The authors declare that they have no competing interests.

Author's contributions

SQZ and HL drafted the manuscript and carried out the experiments. YL designed the experiments. YL and JRZ helped to revise the manuscript. YH and GQH supported the study. All the authors read and approved the final manuscript.

Author's information

[1]State Key Discipline Laboratory of Wide Band Gap Semiconductor Technology, School of Microelectronics, Xidian University, Xi'an 710071, China, *email: xdliuyan@xidian.edu.cn

[§]These authors contribute equally to this work

Availability of Data and Materials

The datasets supporting the conclusions of this article are included in the article.

References

1. Lundstrom MS. The MOSFET revisited: device physics and modeling at the nanoscale. IEEE Int. SOI Conf. 2006;1-3.
2. Sakurai T. Perspectives of low-power VLSI's. IEICE Trans. Electron. 2004;429–436.
3. Sze S, Ng KK. Physics of Semiconductor Devices, 3rd Edition. Wiley Interscience; 2006.
4. Baba T. Proposal for surface tunnel transistors. Jpn. J. Appl. Phys. 1992;31:4.
5. Sarkar D, Xie X, Liu W, et al. A subthermionic tunnel field-effect transistor with an atomically thin channel. Nature. 2015;526:91–95.
6. Gopalakrishnan K, Griffifin P, Plummer J. Impact ionization MOS (IMOS)-Part I: Device and circuit simulations. IEEE Tran. Elec. Dev. 2005;52:69–76.
7. Salahuddin S, Datta S. Use of negative capacitance to provide voltage amplifification for low power nanoscale devices. Nano Lett. 2008;8:405–410.
8. Li KS, Chen PG, Lai TY, et al. Sub-60mV-swing negative-capacitance FinFET without hysteresis. IEEE International Electron Devices Meeting. 2016.
9. Khan AI, Yeung CW, Hu C, et al. Ferroelectric negative capacitance MOSFET: Capacitance tuning & antiferroelectric operation. IEDM Tech Dig. 2011.
10. Salahuddin S, Datta S. Use of negative capacitance to provide voltage amplification for low power nanoscale devices. Nano Letters, 2008;8(2):405-410.
11. Dasgupta S, Rajashekhar A, Majumdar K, et al. Sub-kT/q Switching in Strong Inversion in $PbZr_{52}Ti_{0.48}O_3$ Gated Negative Capacitance FETs. IEEE J Exploratory Solid-State Comput. Devices Circuits. 2017;1:43-48.
12. Bakaul S, Serrao C, Lee M, et al. Single crystal functional oxides on silicon. Nat Commun. 2016;7:10547.
13. Rusu A, Salvatore GA, Jimenez D, et al. Metal-Ferroelectric-Metal-Oxide-Semiconductor Field Effect Transistor with Sub-60mV/decade Subthreshold Swing and Internal Voltage Amplification. Electron Devices Meeting. IEDM Tech Dig. 2010.
14. Jo J, Shin C. Negative Capacitance Field Effect Transistor With Hysteresis-Free Sub-60-mV/Decade Switching. IEEE Electron Device Lett. 2016;37:245-248.
15. Lee MH, Wei YT, Chu KY, et al. Steep Slope and Near Non-Hysteresis of FETs With Antiferroelectric-Like HfZrO for Low-Power Electronics. IEEE Electron Device Lett. 2015;36:294-296.
16. Cheng CH, Chin A. Low-Voltage Steep Turn-On pMOSFET Using Ferroelectric High-k Gate Dielectric. IEEE Electron Device Lett. 2014;35:274-276.

17. Lee MH, Chen PG, Liu C, et al. Prospects for ferroelectric $HfZrO_x$ FETs with experimentally CET=0.98nm, SS_{for}=42mV/dec, SS_{rev}=28mV/dec, switch-OFF <0.2V, and hysteresis-free strategies. IEEE International Electron Devices Meeting. 2015.
18. Müller J, Yurchuk E, Schlsser T, et al. Ferroelectricity in HfO_2 enables nonvolatile data storage in 28 nm HKMG. Symposium on VlSI Technology. 2012.
19. Schroeder U, Yurchuk E, Müller J, et al. Impact of different dopants on the switching properties of ferroelectric hafnium oxide. Jpn J Appl Phys. 2014;53:85-89.
20. Mueller S, Muller J, Schroeder U, et al. Reliability characteristics of ferroelectric Si:HfO_2 thin films for memory applications. IEEE T Device Mat Re. 2013;13:93-97.
21. Park MH, Kim HJ, Kim YJ, et al. Effect of Zr content on the wake-up effect in $Hf_{1-x}Zr_xO_2$ ACS Appl Mater Inter. 2016;8:15466-15475.
22. Schroeder U, Richter C, Park MH, et al. Lanthanum-doped hafnium oxide: a robust ferroelectric material. Inorg Chem. 2018;57:2752-2765.
23. Chernikova AG, Kozodaev MG, Negrov DV, et al. Improved Ferroelectric Switching Endurance of La-Doped $Hf_5Zr_{0.5}O_2$ Thin Films. ACS Appl. Mater. Interfaces. 2018;10:2701-2708.
24. Hyuk PM, Hwan LY, Thomas M, et al. Review and perspective on ferroelectric HfO2-based thin films for memory applications. MRS Comm. 2018;8:795-808.
25. Mueller S, Yurchuk E, Slesazeck S, et al. Performance investigation and optimization of Si:HfO_2 FeFETs on a 28 nm bulk technology. Joint IEEE International Symposium on Applications of Ferroelectric and Workshop on Piezoresponse Force Microscopy. 2013;248-251.
26. Zhou J, Zhou Z, Wang X, et al. Demonstration of Ferroelectricity in Al-doped HfO_2 with a Low Thermal Budget of 500 °C. IEEE Electron Device Lett. 2020;41:1130-1133.
27. Liu H, Peng Y, Han G, et al. ZrO_2 Ferroelectric Field-Effect Transistors Enabled by the Switchable Oxygen Vacancy Dipoles. Nanoscale Res Lett. 2020;15:120.
28. Peng Y, Han G, Liu F, et al. Non-Volatile Field-Effect Transistors Enabled by Oxygen Vacancy Related Dipoles for Memory and Synapse Applications. IEEE Electron Device Lett. 2020.
29. Peng Y, Han G, Liu F, et al. Ferroelectric-like Behavior Originating from Oxygen Vacancy Dipoles in Amorphous Film for Non-volatile Memory. Nanoscale Res Lett. 2020;15:134.
30. Park MH, Kim HJ, Kim YJ, et al. Thin $Hf_xZr_{1-x}O_2$ Films: A New Lead-Free System for Electrostatic Supercapacitors with Large Energy Storage Density and Robust Thermal Stability. Adv Energy Mater. 2014;4:1400610.
31. Schroeder U, Yurchuk E, Mueller J, et al. Impact of different dopants on the switching properties of ferroelectric hafniumoxide. Jpn J Appl Phys. 2014;53:08LE02.
32. Liu H, Peng Y, Han G, et al. ZrO_2 ferroelectric field-effect transistors enabled by the switchable oxygen vacancy dipoles. Nanoscale Research Lett. 2020;15:120.

33. Peng Y, Xiao W, Liu F, et al. Non-volatile field-effect transistors enabled by oxygen vacancy related dipoles for memory and synapse applications. IEEE Electron Device Lett. 2020;67:3632-3636.
34. Peng Y, Han G, Liu F, et al. Ferroelectric-like behavior originating from oxygen vacancy dipoles in amorphous film for non-volatile memory. Nanoscale Research Lett. 2020;5:134.
35. Zhang S, Liu Y, Zhou J, et al. Low Voltage Operating 2D MoS_2 Ferroelectric Memory Transistor with $Hf_{1-x}Zr_xO_2$ Gate Structure. Nanoscale Research Lett. 2020;15:157.
36. Glinchuk MD, Morozovska AN, Lukowiak A, et al. Possible electrochemical origin of ferroelectricity in HfO_2 thin films. J Alloy Compod. 2020;830:153628.
37. Ishibashi Y, Orihara H. A theory of D-E hysteresis loop. Integr Ferroelectr. 1995;9:57-61.
38. Scott JF, Dawber M. Atomic-scale and nanoscale self-patterning in ferroelectric thin films. AIP Conference Proceedings. 2000;535:129.
39. Chen HP, Lee VC, Ohoka A, et al. Modeling and Design of Ferroelectric MOSFETs. IEEE Trans Electron Devices. 2011;58:2401-2405.
40. Zhou J, Peng Y, Han G, et al. Hysteresis reduction in negative capacitance ge pfets enabled by modulating ferroelectric properties in $HfZrO_x$. IEEE J Electron Dev. 2017;6:41-48.
41. Saha AK, Sharma P, Dabo I, et al. Ferroelectric transistor model based on self-consistent solution of 2D Poisson's, non-equilibrium Green's function and multi-domain Landau Khalatnikov equations. IEEE International Electron Devices Meeting. 2018.
42. Zhou J, Han G, Li J, et al. Negative differential resistance in negative capacitance FETs. IEEE Electron Device Lett. 2018;39:622-625.
43. Zhou J, Han G, Li Q, et al. Ferroelectric $HfZrO_x$ Ge and GeSn PMOSFETs with Sub-60 mV/decade subthreshold swing, negligible hysteresis, and improved I_{ds}. IEEE International Electron Devices Meeting. 2017.
44. Sharma P, Tapily K, Saha AK, et al. Impact of total and partial dipole switching on the switching slope of gate-last negative capacitance FETs with ferroelectric hafnium zirconium oxide gate stack. Symposium on VlSI Technology. 2017.
45. Lin L, Robertson J. Atomic mechanism of electric dipole formed at high-K: SiO_2 J Appl Phys. 2011;109:9.
46. Sharia O, Demkov AA, Bersuker G, et al. Theoretical study of the insulator/insulator interface: band alignment at the SiO_2/HfO_2 Phys Rev B. 2007;75:3.
47. Kim G, Kim T, Jeon S. Interfacial Dipole Modulation Device with SiO_X Switching Species. IEEE Electron Device Lett. 2020.

Figures

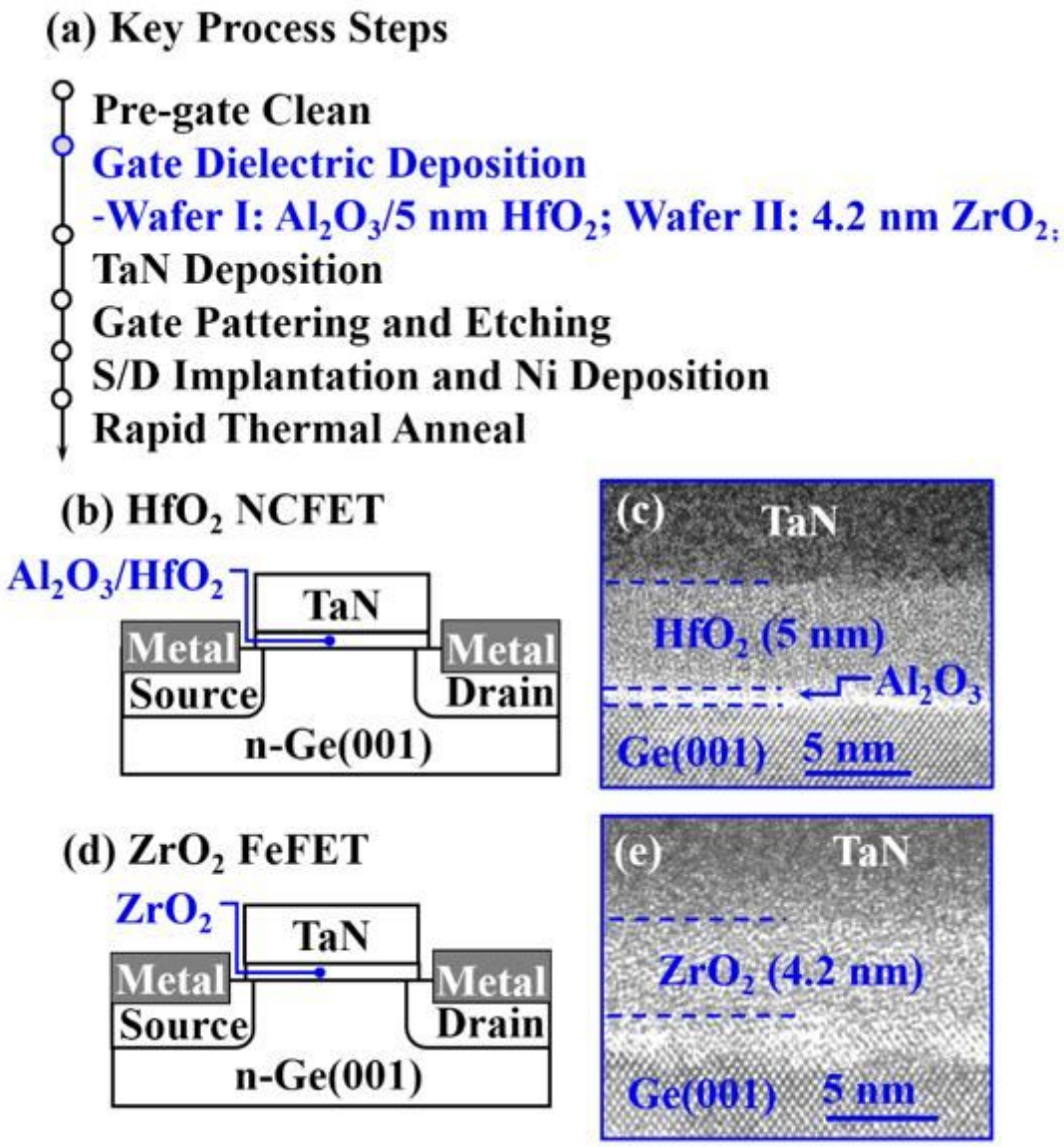


Figure 1

(a) Key process steps for the fabrication of the Al2O3/5 nm HfO2 NCFETs and 4.2 nm ZrO2 NCFETs. (b) Schematics and (c) HRTEM images of the fabricated ZrO2 NCFETs. (d) Schematics and (e) HRTEM images of the fabricated Al2O3/HfO2 NCFETs.

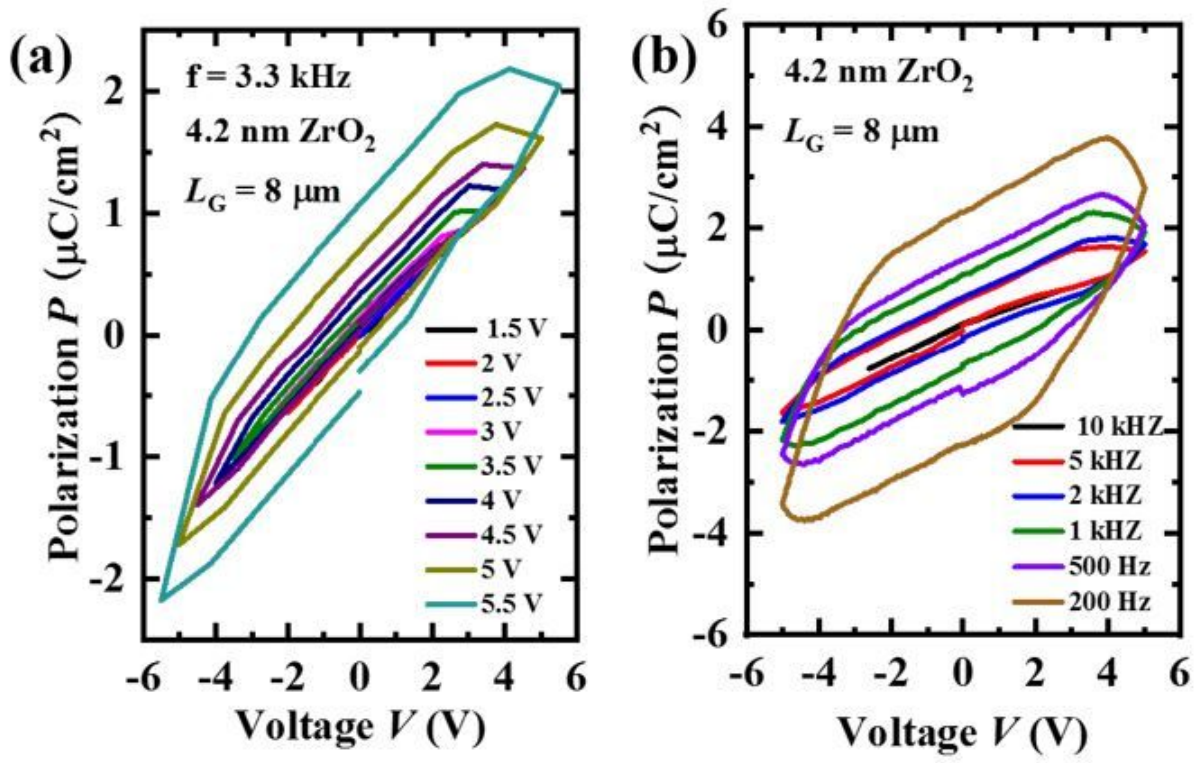


Figure 2

Measured P vs V characteristics of the 4.2 nm ZrO2 capacitors with (a) different sweeping ranges of V and (b) different measurement frequences.

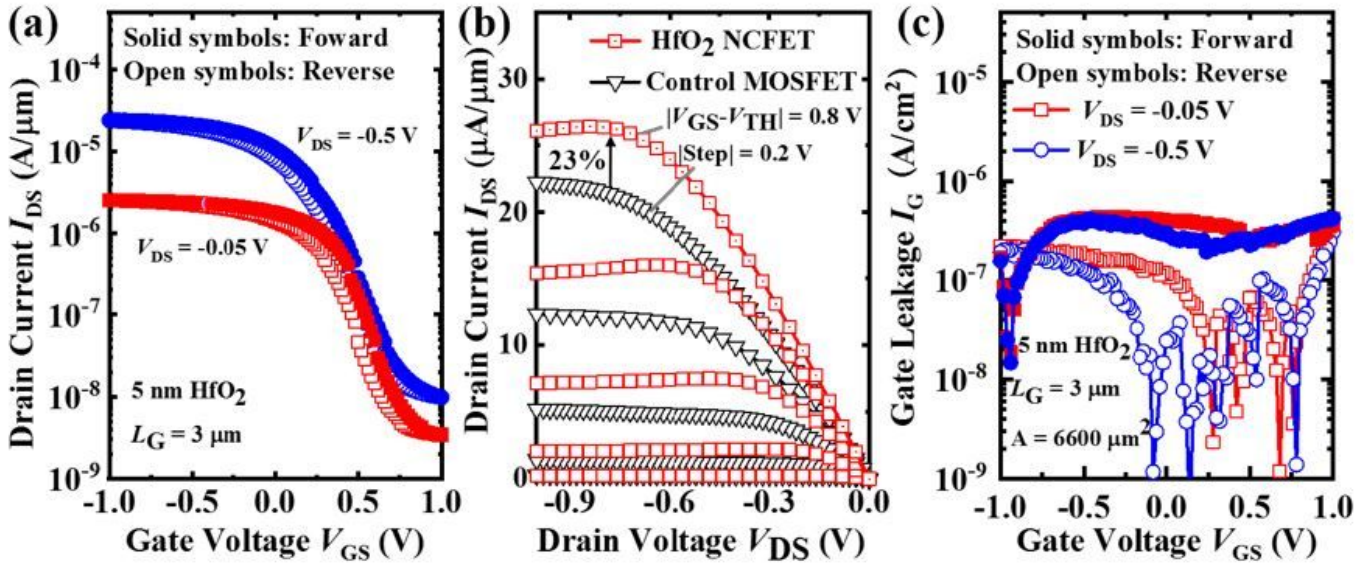


Figure 3

(a) Measured IDS-VGS curves of the 5 nm HfO2 NCFET when VDS = -0.5 V and VDS = -0.05 V. (b) Measured IDS-VDS curves of the HfO2 NCFET and the control MOSFET. (c) Measured IG-VGS curves of the 5 nm HfO2 NCFET when VDS = -0.5 V and VDS = -0.05 V.

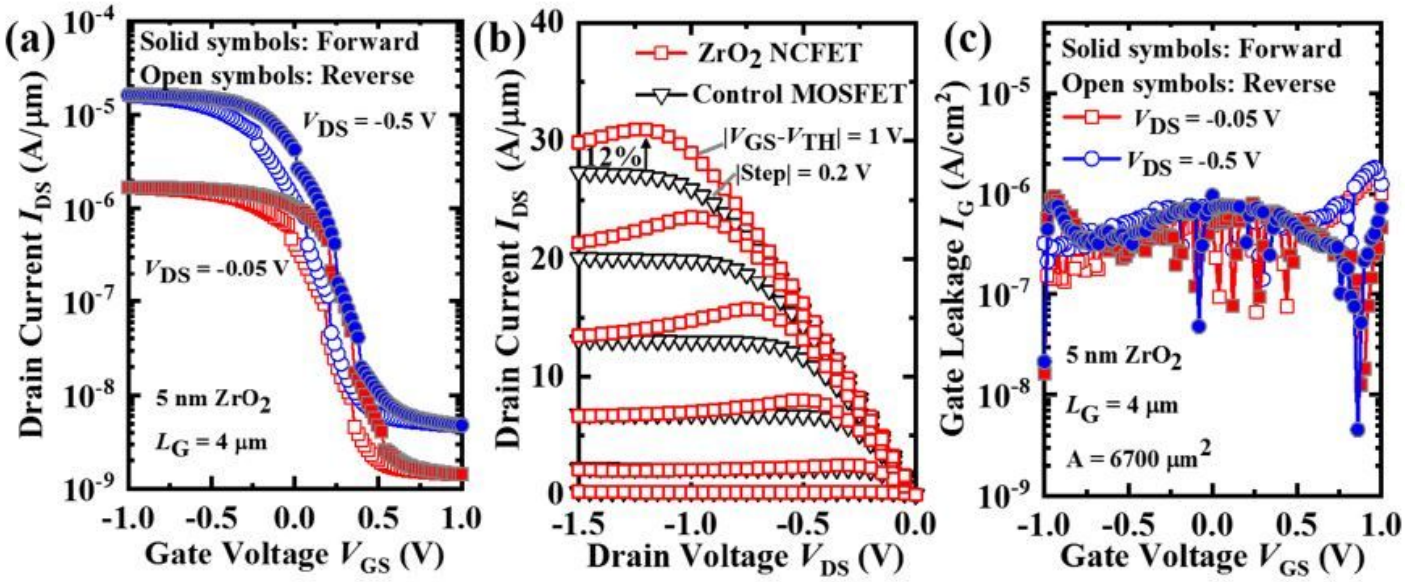


Figure 4

(a) Measured IDS-VGS curves of the 5 nm ZrO2 NCFET when VDS = -0.5 V and VDS = -0.05 V. (b) Measured IDS-VDS curves of the ZrO2 NCFET and the control MOSFET demonstraing the obvious NDR phenomenon. (c) Measured IG-VGS curves of the 5 nm ZrO2 NCFET when VDS = -0.5 V and VDS = -0.05 V.

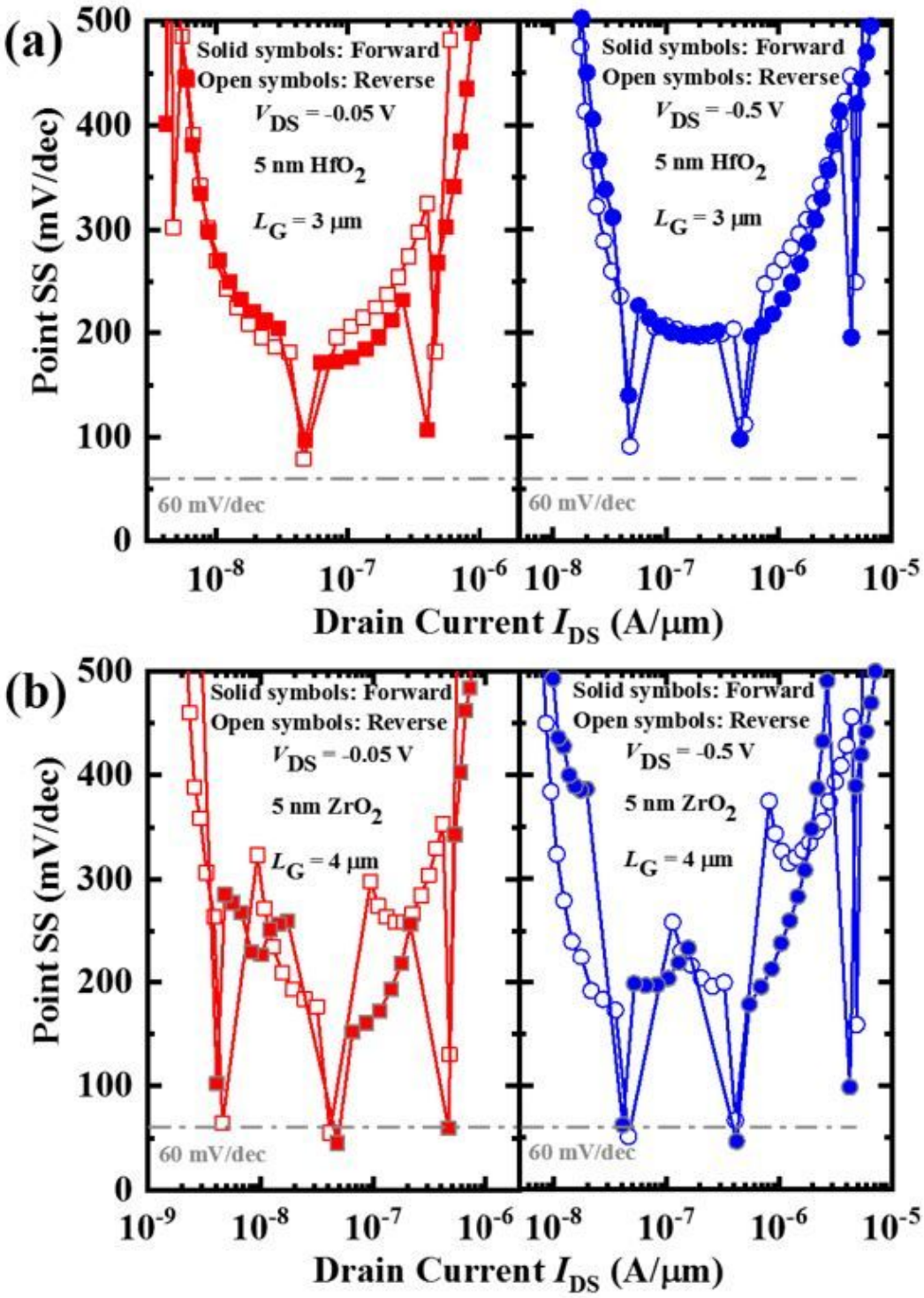


Figure 5

Point SS as a function of IDS for the (a) Al2O3/5 nm HfO2 NCFETs and (b) 5 nm ZrO2 NCFETs.